Hindawi
Mathematical Problems in Engineering
Volume 2022, Article ID 3166926, 10 pages
https://doi.org/10.1155/2022/3166926

Research Article

Position Control of a Single-Rod Electro-Hydrostatic Actuator Experiencing a Leaky Piston Seal

Guangan Ren[1], **Xiangwei Mou**[2], **Xiaohao Wen**[2], **and Lintao Chen**[2]

[1]*College of Intelligence Science and Technology, National University of Defense Technology, Changsha 410073, China*
[2]*Teachers College for Vocational and Technical Education, Guangxi Normal University, Guilin 541004, China*

Correspondence should be addressed to Xiangwei Mou; xwmou@mailbox.gxnu.edu.cn

Received 28 May 2022; Revised 30 June 2022; Accepted 17 August 2022; Published 15 September 2022

Academic Editor: Xingling Shao

Single-rod cylinders are generally employed in electro-hydrostatic actuators (EHAs). A condition that is difficult to detect and could degrade the performance in single-rod EHAs, is the faulty cylinder piston seal. It causes internal leakage from one chamber of the actuator to another. In this work, a position controller with tolerance to actuator internal leakage is synthesized for a single-rod EHA using quantitative feedback theory (QFT). The controller is also robust to different loading and environmental stiffnesses. The ability of the controller is compared with another QFT controller that is synthesized without considering leakage fault. The simulation results show that the QFT fault-tolerant controller can meet prescribed specifications despite internal leakage up to 8.6 L/min.

1. Introduction

An electro-hydrostatic actuator (EHA) is pump-controlled that has already been used for aircrafts [1], vehicles [2], and manipulators [3, 4]. In the literature, a double-rod cylinder is often used in an EHA system and its circuit structure is simple. However, single-rod EHAs with four possible circuit configurations have more potential applications [5, 6]. Single-rod EHAs can suffer from various faults. In particular, a leaky piston seal can cause internal leakage from one chamber of the actuator to another that can degrade system performance. In order to compensate for the adverse effects caused by faults, fault-tolerant control (FTC) methods are widely utilized. FTC schemes can be divided into two groups, namely, active and passive FTC. In the former, the controller is adaptive and alters online as faults happen. In the latter, a robust controller is designed that is insensitive to faults in closed-loop performance [7–11]. This type of controllers is preferable due to its simple structure and easy application.

Quantitative feedback theory (QFT) is a robust linear controller design method. During the controller design process, performance specifications, parametric uncertainties, and controller structure can be balanced [12, 13]. QFT controllers have been successfully applied to deal with internal leakage fault. Karpenko and Sepehri [14] developed an active QFT-based FTC scheme, and they further designed passive QFT fault-tolerant controllers [15, 16]. All these controllers were implemented on valve-controlled systems. Ren et al. [17–20] synthesized QFT position and QFT actuating pressure controllers despite leakage. These controllers were developed for double-rod EHAs. Apart from QFT, an adaptive backstepping technique developed by Chen and Liu [21] has been proposed to deal with internal leakage. This system is not an EHA because directional valves were used to control the flow. Maddahi et al. [22] developed a fractional-order PID fault-tolerant controller for a valve-controlled system. Moghaddam et al. [23] combined fractional-order PID controllers and a fuzzy inference system to accommodate internal leakage for a single-rod EHA. However, this active FTC strategy necessitates a fault detection algorithm. The contribution of the work is to design of a passive FTC scheme for a single-rod EHA that is tolerant to internal leakage fault et al. l four quadrants. The system includes various load masses, environmental stiffnesses, and other uncertainties. The novelties are (1) the development of a robust fault-tolerant controller despite cross port leakage for a single-rod EHA, (2) the establishment of the mathematical model for the system considering leakage fault, and (3) the performance comparison of the fault-tolerant controller and the one designed for normal operation (no leak).

The remainder of this paper is organized as follows: mathematical model of the system is described in Section 2. Section 3 shows the development of a QFT fault-tolerant controller and QFT normal controller. Section 4 examines the performances of the two QFT controllers in simulations. Conclusions are provided in Section 5.

2. Modeling

The novel single-rod EHA circuit developed by Costa and Sepehri [6] is used for this study. Its schematic is shown in Figure 1. The system includes a bidirectional main pump, a servomotor, an auxiliary pump, a relief valve, a single-rod cylinder, a load mass, a spring, a one-directional flow control valve, and a three-position four-way directional valve. The settling pressure of a relief valve (item 4) is 5.5×10^5 Pa. The working principle of the system is described in [6, 24]. When the load pressure p_L ($p_L = p_a\text{-}A_b p_b/A_a$) > 0, the solenoid y of V2 is energized, and when $p_L < 0$, the solenoid z is energized. The four quadrants of the system is shown in Figure 2.

From Figure 1, the flow equation of the main pump is

$$\mathrm{Q}_1 = \mathrm{Q}_2 = \omega_\mathrm{m}\mathrm{V}_\mathrm{d}. \tag{1}$$

The flows out of and into the pump are represented by Q_1 and Q_2, respectively; ω_m is the speed of the servo motor; the pump displacement is represented by V_d. The speed of the servo motor is [17].

$$\dot{\omega_m} = \tau_m\left(\left(-\omega_m\right) + \left(K_m u\right)\right). \tag{2}$$

Here, K_m represents the servomotor gain; τ_m represents the time constant of the motor; u is used as input voltage to the motor. The actuator area ratio is

$$\alpha = \frac{A_b}{A_a}, \tag{3}$$

where A_a and A_b are the area of the piston at the cab side and the rod side, respectively. The load pressure is

$$p_L = p_a - \alpha p_b, \tag{4}$$

where p_a and p_b are the chamber pressures of the actuator. The continuity equations are

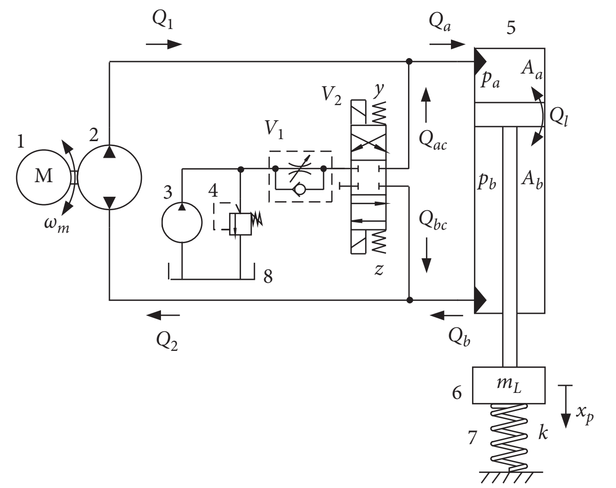

Figure 1: Schematic of the system developed in [6]. 1: Servomotor. 2: Bidirectional pump.3: Auxiliary pump. 4: Relief valve. 5: Actuator. 6: Load mass. 7: Spring. 8: Tank. V1: One-directional flow control valve. V2: Three-position four-way directional valve.

$$\begin{aligned} Q_1 + Q_{ac} &= Q_a, \\ &= A_a\dot{x_p} + \left(\frac{\left(V_{oa}\right) + \left(A_a x_p\right)}{\beta_e}\right)\dot{p_a} + Q_l, \end{aligned} \tag{5}$$

$$\begin{aligned} Q_{bc} - Q_2 &= -Q_b, \\ &= -A_b\dot{x_p} + \left(\frac{\left(V_{ob}\right) - \left(A_b x_p\right)}{\beta_e}\right)\dot{p_b} - Q_l, \end{aligned} \tag{6}$$

where Q_{ac} and Q_{bc} are flows from the auxiliary circuit; Q_a and Q_b are the flows into and out of the actuator, respectively; x_p and $\dot{x_p}$ are the actuator position and velocity, respectively; β_e is the effective bulk modulus of the fluid; V_{oa} and V_{ob} are actuator chamber volumes at the two sides, respectively. The internal leakage Q_l is constructed as follows [17]:

$$Q_l = K_i\left(p_a - p_b\right). \tag{7}$$

In (7), K_i is the coefficient of the internal leakage. For single-rod actuators, the following assumption can be used [25,26].

$$\frac{\left(V_{oa}\right) + \left(A_a x_p\right)}{\beta_e} \approx \frac{\left(V_{ob}\right) - \left(A_b x_p\right)}{\beta_e} \approx \frac{\left(V_{oa}\right) + \left(V_{ob}\right)}{2\beta_e} = C, \tag{8}$$

where C is the hydraulic compliance. The dynamic equation of the piston is

$$\left(m_{rod} + m_L\right)\ddot{x_p} = A_a p_L - f\dot{x_p} + F_L. \tag{9}$$

In (9), $\ddot{x_p}$ is actuator acceleration; m_{rod} is the piston and the rod mass; m_L is the load mass; f is the viscous damping coefficient; the load force F_L is

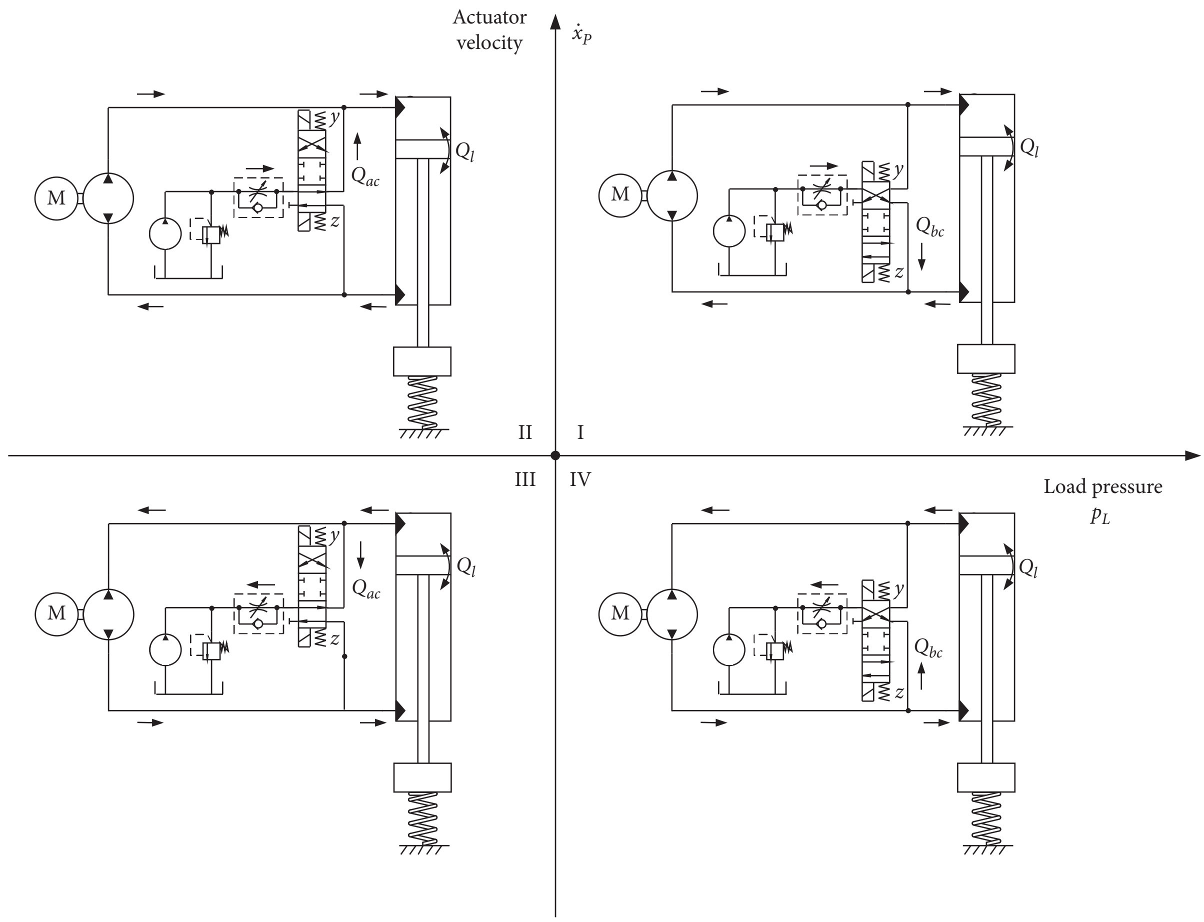

Figure 2: Four-quadrant operation of the system developed in [6].

$$F_L = (m_{rod} + m_L)g - kx_p, \tag{10}$$

where g is the gravitational acceleration; k is the stiffness of the environment.

When the actuator is extending ($\dot{x}_p > 0$), the auxiliary pump provides flow into one side of the actuator through V1 (Quadrants I and II in Figure 2). The following equation can be obtained:

$$Q_b - Q_l = \alpha (Q_a - Q_l). \tag{11}$$

From Equations (3) to (8) and (11), the following equations can be obtained:

$$\left(1 + \alpha^2\right) Q_a = \left(1 + \alpha^2\right) A_a \dot{x}_p + C\dot{p}_L + (1 + \alpha) K_i p_L, \tag{12}$$

$$\left(1 + \alpha^2\right) Q_b = \alpha \left(1 + \alpha^2\right) A_a \dot{x}_p + C\alpha \dot{p}_L + (1 + \alpha) K_i p_L. \tag{13}$$

In Quadrant I, $p_L > 0$ and $Q_{ac} = 0$. Performing Laplace transformation of Equations (1), (2), (5), (9), (10), and (12), the following plant transfer function $P_1(s)$ can be obtained:

$$\begin{aligned} P_1(s) &= \frac{X_p(s)}{U(s)}, \\ &= \frac{\left(1 + \alpha^2\right) A_a V_d \tau_m K_m}{(s + \tau_m)\left[(m_{rod} + m_L) C s^3 + B_1 s^2 + A_1 s + (1 + \alpha) k K_i\right]}, \end{aligned} \tag{14}$$

where the constant A_1 and B_1 are

$$\begin{aligned} A_1 &= kC + (1 + \alpha) f K i + \left(1 + \alpha^2\right) A_a^2, \\ B_1 &= fC + (1 + \alpha)(m_{rod} + m_L) K_i. \end{aligned} \tag{15}$$

In Quadrant II, $p_L < 0$ and $Q_{bc} = 0$. The plant model $P_2(s)$ can be got using Equations (1), (2), (6), (9), (10), and (13):

$$\begin{aligned} P_2(s) &= \frac{X_p(s)}{U(s)}, \\ &= \frac{\left(1 + \alpha^2\right) A_a V_d \tau_m K_m}{(s + \tau_m)\left[\alpha (m_{rod} + m_L) C s^3 + B_2 s^2 + A_2 s + (1 + \alpha) k K_i\right]}, \end{aligned} \tag{16}$$

where the constant A_2 and B_2 are

$$A_2 = \alpha kC + (1+\alpha) fKi + \alpha\left(1+\alpha^2\right)A_a^2,$$
$$B_2 = \alpha fC + (1+\alpha)\left(m_{rod} + m_L\right)K_i. \tag{17}$$

When the actuator is retracting ($\dot{x}_p$ <0), the oil flows from one chamber of the actuator to the tank (Quadrants III and IV in Figure 2).

In Quadrant III, $p_L < 0$ and $Q_{bc} = 0$, Q_{ac} is [24].

$$Q_{ac} = -K_a p_a, \tag{18}$$

where K_a is the pressure sensitivity gain. Using Equations (1) to (10) together with (18), the plant model $P_3(s)$ can be obtained as follows:

$$P_3(s) = \frac{X_p(s)}{U(s)},$$
$$= \frac{[(1+\alpha)Cs + \alpha K_a]A_a V_d \tau_m K_m}{(s+\tau_m)\left[(m_{rod}+m_L)C^2 s^4 + C_3 s^3 + B_3 s^2 + A_3 s + kK_a K_i\right]}, \tag{19}$$

where the constant A_3, B_3, and C_3 are

$$A_3 = fK_aK_i + 2kCK_i + kCK_a + (1-\alpha)^2 {A_a}^2 K_i + \alpha^2 {A_a}^2 K_a,$$
$$B_3 = (m_{rod}+m_L)K_aK_i + 2fCK_i + fCK_a + kC^2 + \left(1+\alpha^2\right)C{A_a}^2,$$
$$C_3 = 2(m_{rod}+m_L)CK_i + (m_{rod}+m_L)CK_a + fC^2. \tag{20}$$

In Quadrant IV, $p_L > 0$ and $Q_{ac} = 0$, Q_{bc} is [24].

$$Q_{bc} = -K_b p_b, \tag{21}$$

where K_b is the pressure sensitivity gain. Using Equations (1) to (10) together with (21), the plant model $P_4(s)$ is

$$P_4(s) = \frac{X_p(s)}{U(s)},$$
$$= \frac{[(1+\alpha)Cs + K_b]A_a V_d \tau_m K_m}{(s+\tau_m)\left[(m_{rod}+m_L)C^2 s^4 + C_4 s^3 + B_4 s^2 + A_4 s + kK_b K_i\right]}, \tag{22}$$

where the constant A_4, B_4, and C_4 are

$$A_4 = fK_bK_i + 2kCK_i + kCK_b + (1-\alpha)^2 {A_a}^2 K_i + {A_a}^2 K_b,$$
$$B_4 = (m_{rod}+m_L)K_bK_i + 2fCK_i + fCK_b + kC^2 + \left(1+\alpha^2\right)C{A_a}^2,$$
$$C_4 = 2(m_{rod}+m_L)CK_i + (m_{rod}+m_L)CK_b + fC^2. \tag{23}$$

The system includes the above four cases and is hereby the system model is expressed as $P(s) \in \{P_1(s), P_2(s), P_3(s), P_4(s)\}$. The internal leakage coefficient K_i and spring stiffness k change the plant type. Table 1 lists the parameter values [24] of the system. The minimum value of K_i is 0, which represents a healthy piston seal. The maximum value of K_i is prescribed to represent the most severe piston faulty condition. Note that, the uncertainty range of m_L and k are also considered to ensure that both resistive and assistive load forces can be generated. These parameters are used in the simulations.

Table 1: Parameter values of the single-rod electro-hydrostatic actuator.

Symbol	Value	
	Nominal	Range
V_d	8×10^{-6}	—
τ_m	3	2.3–4.0
K_m	5.8	5.6–6.0
A_a	3167×10^{-6}	—
A	0.75	—
K_i	—	$0–2.4 \times 10^{-11}$
β_e	689×10^6	$356 \times 10^6–1030 \times 10^6$
C	3.46×10^{-12}	$2.20 \times 10^{-12}–7.03 \times 10^{-12}$
m_{rod}	10	9–11
m_L	—	0–300
F	900	600–1200
K	—	$0–130 \times 10^3$
K_a, K_b	4.65×10^{-10}	$2.08 \times 10^{-10}–4.65 \times 10^{-10}$

3. QFT Controller Design

Figure 3 shows the schematic of the control system [13]. As per prescribed specifications, a controller G and a prefilter F have to be synthesized despite uncertainties in the plant P.

3.1. Plant Templates. Parametric uncertainties of the plant (shown in Table 1) are captured by templates in the frequency domain on the Nichols chart. Template sizes are influenced by the effects of uncertainties on the plant. The templates of the plant $P(s)$ for normal operation ($K_i = 0$) and the ones considering internal leakage ($K_i \geq 0$) are shown in Figures 4(a) and 4(b), respectively. Note that internal leakage increases templates sizes at low frequencies. It introduces phase variation with a maximum value of 90 degree and a magnitude variation. The larger templates make it hard to design the controller.

3.2. Prescribed Specifications

3.2.1. Tracking Specification. The uncertain plant P(s) is expressed as $P(s, \beta)$, where the vector $\beta = [\tau_m, K_m, f, C, m_{rod}, m_L, K_i, k, K_a, K_b]^T$. With reference to Figure 3, the transfer function of the closed-loop system $T(s, \beta)$ is

$$T(s,\beta) = F(s)\frac{G(s)P(s,\beta)}{1+G(s)P(s,\beta)}, \tag{24}$$

where G(s) represents the QFT controller for normal operation G_N(s) or the QFT fault-tolerant controller G_{FTC}(s); F(s) is the prefilter designed for G_N(s) or G_{FTC}(s). The tracking requirement is shown as follows:

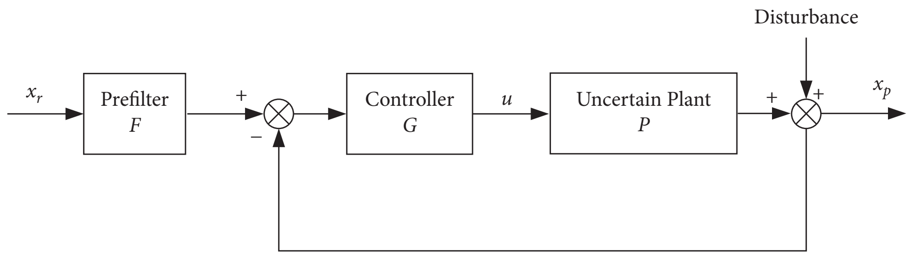

Figure 3: Schematic of the QFT control system.

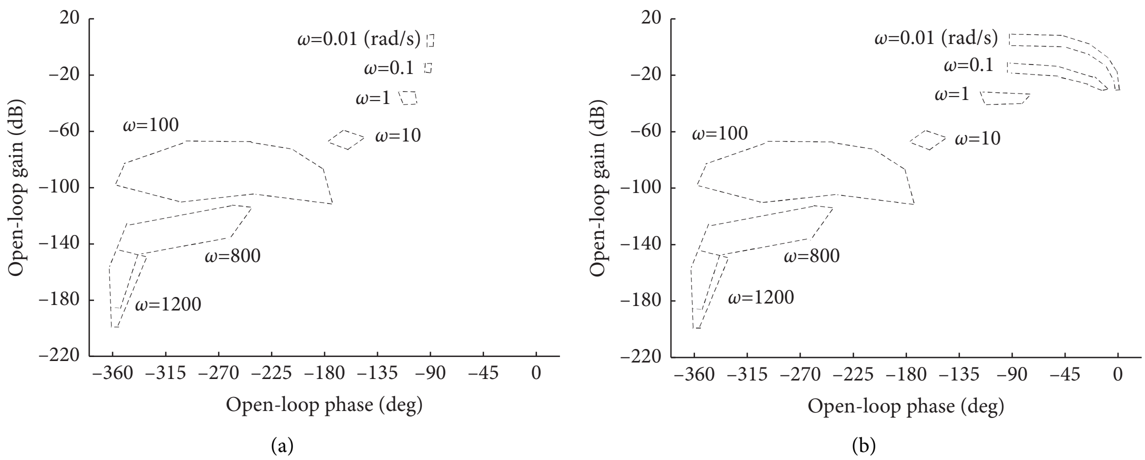

Figure 4: Templates of the uncertain plant (P) (a) for normal operation and (b) considering actuator internal leakage.

$$\begin{aligned} &\left| T_L(j\omega) = \frac{1}{((1/0.5s)+1)(s+1)((1/5s)+1)((1/30s)+1)((1/200s)+1)^2} \right| \\ &\leq |T(j\omega,\boldsymbol{\beta})| \leq \left| T_U(j\omega) = \frac{(1/0.55s)+1}{((1/0.9s)+1)(s+1)^2} \right| \quad \forall \boldsymbol{\omega} \in [0\,\infty), \end{aligned} \tag{25}$$

where $T_U(s)$ is the upper tracking bound and $T_L(s)$ is the lower tracking bound. According to (25), the frequency responses of $T(s, \boldsymbol{\beta})$ should be within the above-given two tracking bounds.

3.2.2. Stability Specification. The stability specification is [13]

$$\left| \frac{G(j\omega)P(j\omega,\beta)}{1+G(j\omega)P(j\omega,\beta)} \right| \leq 1.6\ (4.1\,dB) \quad \forall \boldsymbol{\omega} \in [0\ \infty), \tag{26}$$

(26) ensures a gain margin of 4.22 dB and a phase margin of 36.42° [17, 18].

3.2.3. Sensitivity Specification. The following equation needs to be satisfied for disturbance rejection:

$$\left| \frac{1}{1+G(j\omega)P(j\omega,\beta)} \right| \leq 1.8\ (5.1\,dB) \quad \forall \boldsymbol{\omega} \in [0\,\infty). \tag{27}$$

3.3. Loop Shaping and Prefilter Design. A nominal plant $P(j\omega, \boldsymbol{\beta_0})$ is selected by using a set of parameters in $P(j\omega, \boldsymbol{\beta})$. It is then employed to calculate QFT bounds together with the above-prescribed specifications and plant templates on the Nichols chart. The controller is designed by shifting the nominal plant $P(j\omega, \boldsymbol{\beta_0})$ until the nominal loop transmission $L(j\omega, \boldsymbol{\beta_0}) = G(j\omega)\ P(j\omega, \boldsymbol{\beta_0})$ satisfies QFT bounds et al.l selected frequencies. The bounds are either open or closed. In order to satisfy these bounds, $L(j\omega, \boldsymbol{\beta_0})$ should be above the open bounds and outside closed bounds at the corresponding frequencies on the Nichols chart.

Figure 5(a) shows the QFT bounds and a suitable loop transmission for normal operation ($K_i = 0$). In order to satisfy open bounds, a small gain is employed in the controller. The next two poles are also added to satisfy closed bounds at high frequencies. The normal controller is shown in the following equation:

$$G_N(s) = \frac{50}{((1/6s)+1)((1/6s)+1)}. \tag{28}$$

When the internal leakage is considered ($K_i \geq 0$), the QFT bounds and a suitable loop transmission are shown in

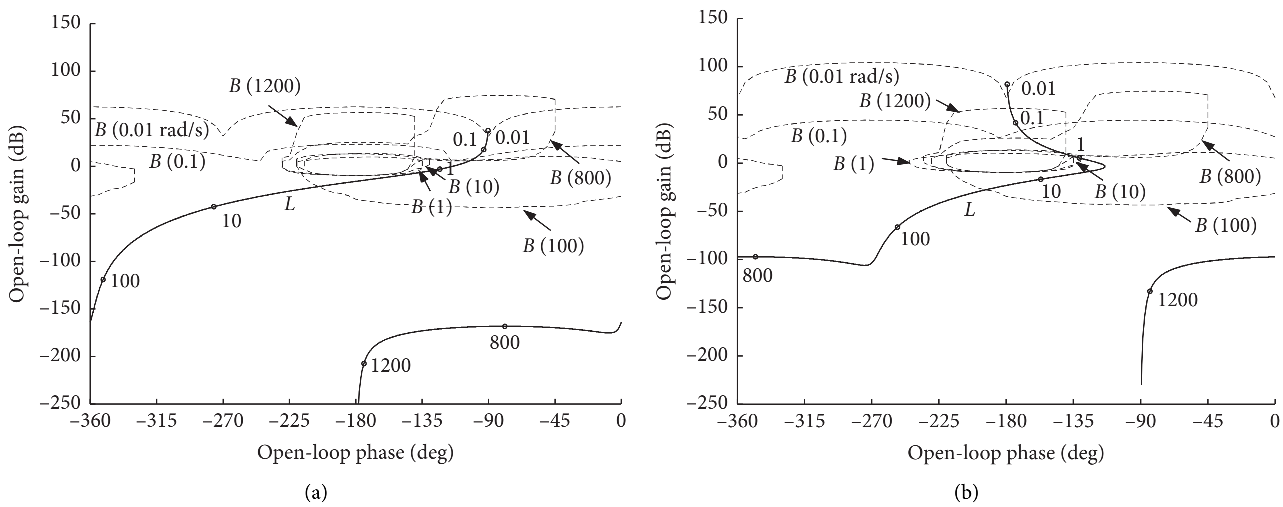

Figure 5: QFT bounds (B) (ω) and nominal loop transmission (L) (jω, β0) (a) for normal operation and (b) considering actuator internal leakage.

Figure 5(b). An integrator is added in the fault-tolerant controller to make $L(j\omega, \boldsymbol{\beta_0})$ satisfy QFT bound requirements with a smaller controller bandwidth. Next, the open-loop gain is increased to meet open bounds. Finally, two zeros and two poles are used in the controller to satisfy closed bounds at intermediate frequencies and high frequencies, respectively. The designed fault-tolerant controller is shown in the following equation:

$$G_{FTC}(s) = \frac{80(s+1)((1/2s)+1)}{s((1/10s)+1)((1/20s)+1)}. \tag{29}$$

By observing (28), an integrator, a high open-loop gain, and two zeros are needed in the fault-tolerant controller to cope with internal leakage fault. The ratio of controller gains $|G_{FTC}(s)|/|G_N(s)|$ is also calculated to further ascertain the price, as shown in Figure 6. It is seen that the integrator part in $G_{FTC}(s)$ introduces extra gain at low frequencies ($\omega < 1$ rad/s) to remove static errors caused by leakage. At the intermediate-frequency band (1 rad/s$\leq \omega \leq 10$ rad/s), two zeros of $G_{FTC}(s)$ leads to over 8 dB ratio, that is required to satisfy its QFT bounds. Although the magnitude of $G_{FTC}(s)$ is much higher than that of $G_N(s)$ (ratio >25 dB) at high frequencies ($\omega > 10$ rad/s), which indicates $G_{FTC}(s)$ is more susceptible to noise and unmodelled high-frequency dynamics, the prescribed specifications are still satisfied for both controllers.

Loop shaping just ensures the satisfactions of Equations (26), (27), and (30), therefore a prefilter was synthesized to meet (25). The prefilter can make closed-loop frequency responses within upper and lower QFT tracking bounds. The prefilter designed for normal operation and the one synthesized considering internal leakage are given by (31), respectively. Both prefilters have the same number of zeros and poles.

$$20\log_{10}|T(j\omega,\beta)|_{max} - 20\log_{10}|T(j\omega,\beta)|_{min} \leq 20\log_{10}|T_U(j\omega)| - 20\log_{10}|T_L(j\omega)|, \tag{30}$$

$$F_N(s) = \frac{((1/2s)+1)((1/4s)+1)((1/150s)+1)}{((1/0.5s)+1)((1/30s)+1)((1/500s)+1)}, \tag{31}$$

$$F_{FTC}(s) = \frac{((1/5s)+1)((1/5s)+1)((1/180s)+1)}{((1/0.5s)+1)(1/1.5s+1)((1/15s)+1)}. \tag{32}$$

4. Simulation Studies

The designed two QFT controllers were examined under normal operation (no leak) and leaky operation, respectively. Their ability to satisfy tracking bounds was shown in simulations. The ranges of parameters listed in Table 1 were also considered.

In the first test, the nominal system was operated under normal operation. A load of 300 kg and a spring of 130 kN/m was chosen as the load force. Simulation results for the normal controller G_N and fault-tolerant controller G_{FTC} are shown in Figures 7 and 8, respectively. As is seen, the actuator position responses of the two controllers are within tracking bounds. In addition, when the quadrant switches, the control signal of G_{FTC} is more oscillatory than that of G_N. This is because the bandwidth of G_{FTC} is higher, making it more sensitive to the changes and disturbances of the system.

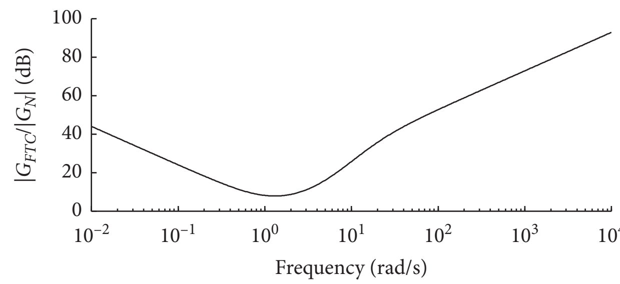

Figure 6: Ratio of controller gains $|G_{FTC}|/|G_N|$.

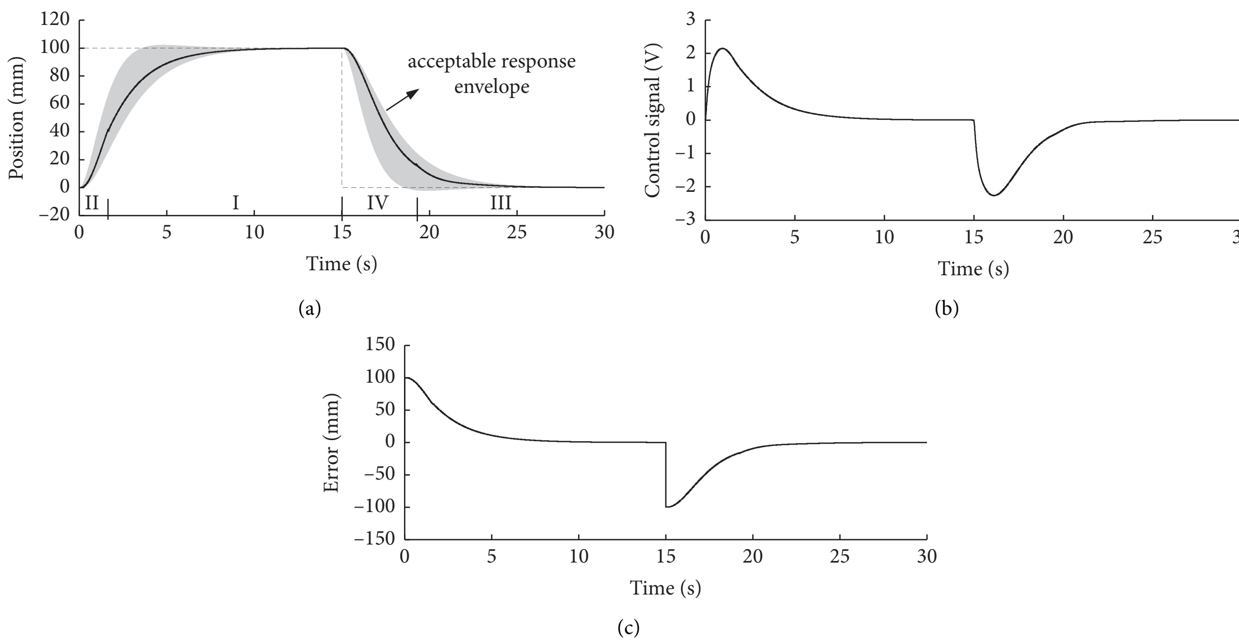

Figure 7: Simulation responses of QFT controller G_N and F_N to a 100-mm step input for actuator working under normal (no leak) condition, pushing against a 130 kN/m spring and moving a load mass of 300 kg. (a) Position. (b) Control signal. (c) Position error.

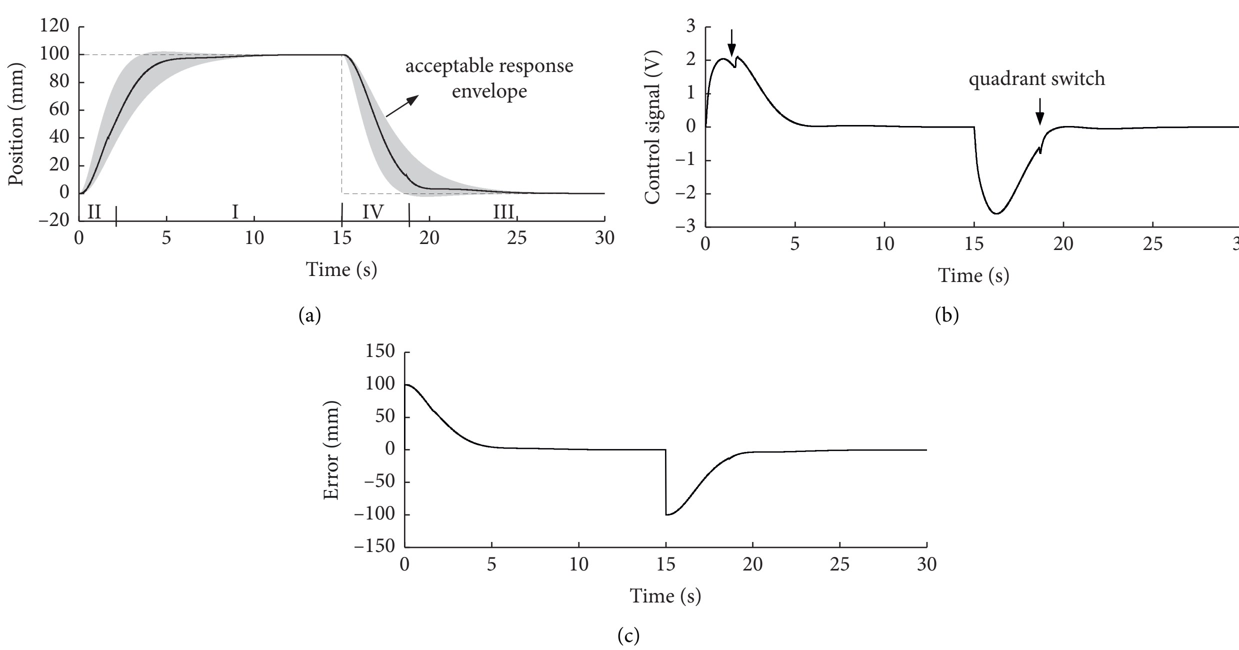

Figure 8: Simulation responses of QFT controller G_{FTC} and F_{FTC} to a 100-mm step input for actuator working under normal (no leak) condition, pushing against a 130 kN/m spring and moving a load mass of 300 kg. (a) Position. (b) Control signal. (c) Position error.

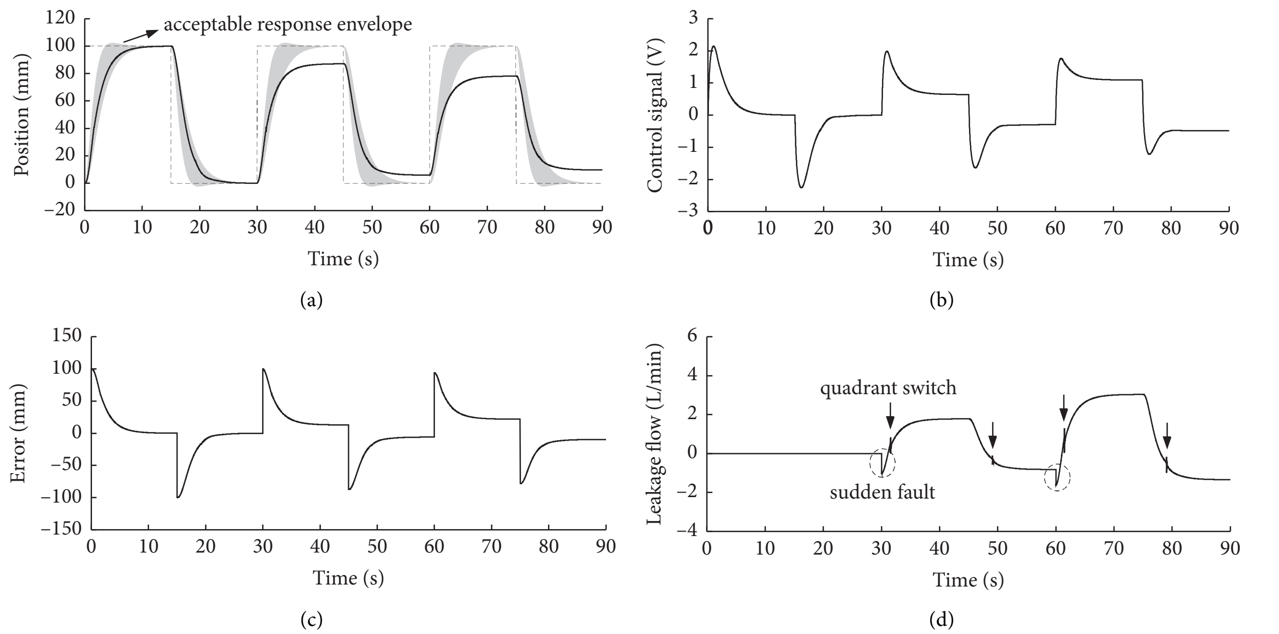

Figure 9: Simulation responses of QFT controller G_N and F_N to a 100-mm square-wave input for actuator working against a 130 kN/m spring and moving a load mass of 300 kg in the presence of increasing leakage flow. (a) Position. (b) Control signal. (c) Position error. (d) Leakage flow.

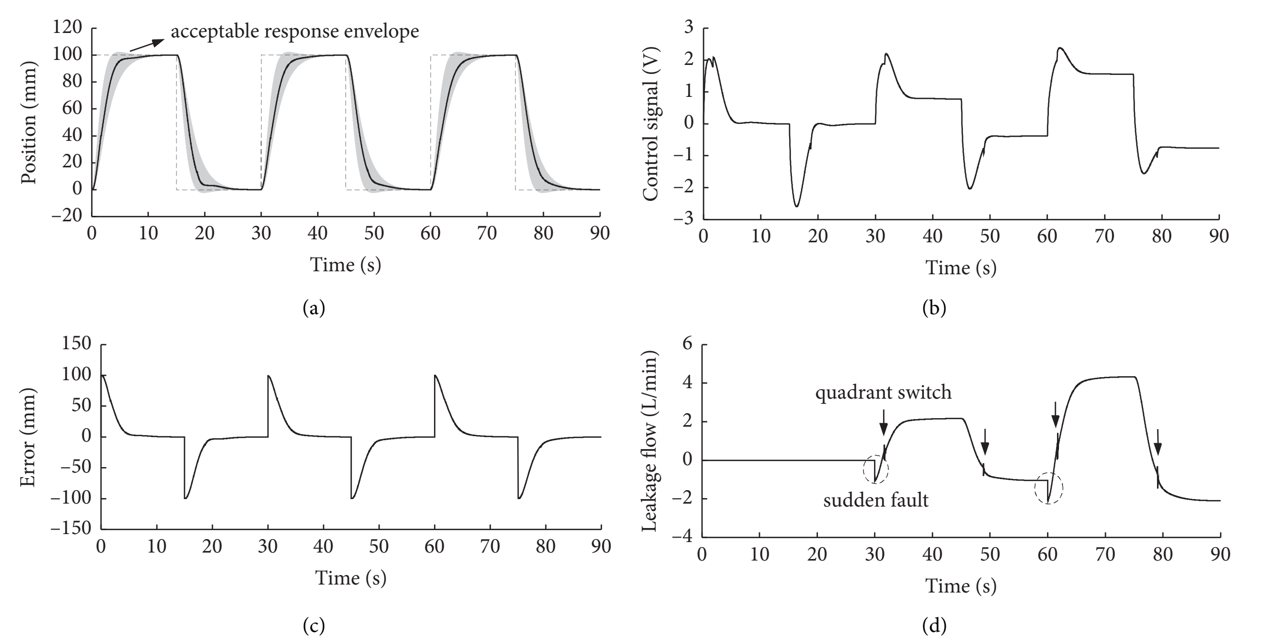

Figure 10: Simulation responses of QFT controller G_{FTC} and F_{FTC} to a 100-mm square-wave input for actuator working against a 130 kN/m spring and moving a load mass of 300 kg in the presence of increasing leakage flow. (a) Position. (b) Control signal. (c) Position error. (d) Leakage flow.

Next, internal leakage was gradually introduced (K_i increases from 0 to its maximum value) to evaluate the performance of the two controllers in leaky operation. The responses of G_N and G_{FTC} to a 100-mm square-wave input are shown in Figures 9 and 10, respectively. It is seen that the steady-state error of G_N increases with leakage and finally the tracking specification is violated. On the other hand, the position response of G_{FTC} satisfies tracking bounds, even when leakage increases to 4.4 L/min.

Finally, G_{FTC} was tested under various leakage levels (K_i increases from 0 to $2.4 \times 10^{-11}\,\mathrm{m}^3/(\mathrm{s}\cdot\mathrm{Pa})$), step inputs (50 mm, 100 mm, and 150 mm), load masses (0 kg, 150 kg, and 300 kg), and environmental stiffnesses (0 kN/m, 65 kN/m, and 130 kN/m). Parametric uncertainties in Table 1 were also considered. With reference to Figure 11, tracking bounds are satisfied even if leakage increases to 8.6 L/min.

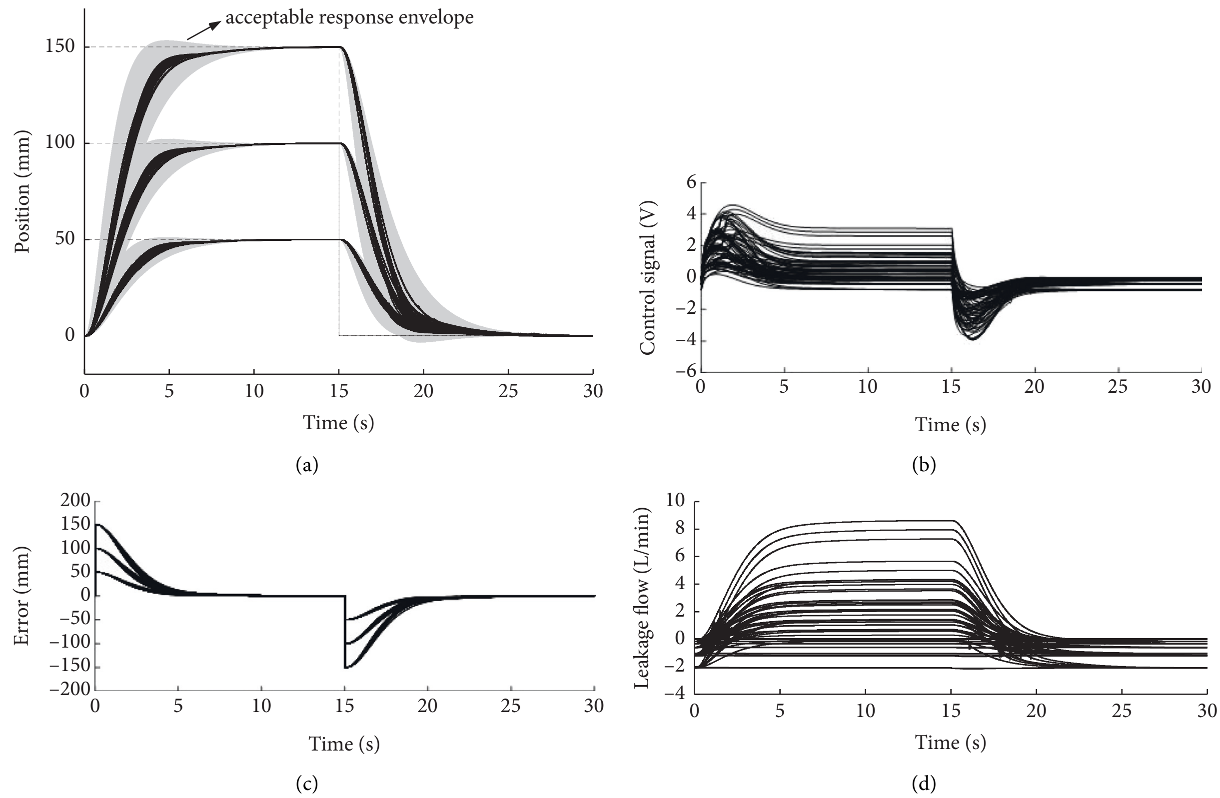

FIGURE 11: Simulation responses of QFT controller G_{FTC} and F_{FTC} to various step inputs for normal operation as well as different leakage levels, considering parameter ranges in Table 1 the actuator is moving load masses of 0 kg, 150 kg, and 300 kg in free motion, against a 65- and 130-kN/m spring. (a) Position. (b) Control signal. (c) Position error. (d) Leakage flow.

5. Conclusions

A fault-tolerant controller was synthesized for a single-rod EHA. The controller required an integrator, a high open-loop gain, and two zeros to compensate for leakage flow. Another QFT controller was also designed under normal operation (no leak). Simulation results demonstrated that the QFT fault-tolerant controller was capable of maintaining actuator responses within tracking bounds despite internal leakage up to 8.6 L/min. However, the QFT normal controller could not satisfy the prescribed specifications if internal leakage occurred.

Data Availability

The data used to support the findings of this study are available from the corresponding author upon request.

Conflicts of Interest

The authors declare that there are no conflicts of interest regarding the publication of this paper.

Acknowledgments

This work was supported in part by Hunan Provincial Natural Science Foundation of China under Grant no. 2022JJ40550, in part by the National Natural Science Foundation of China under Grant no. 52105077, and in part by the Guangxi Natural Science Foundation under Grant no. 2018GXNSFAA050026.

References

[1] S. C. Jensen, G. D. Jenney, and D. Dawson, "Flight test experience with an electromechanical actuator on the F-18 systems research aircraft," in *Proceedings of the 19th IEEE Digital Avionics Systems Conference*, pp. 7–13, Philadelphia, PA, USA, October 2000.

[2] T. B. Miller, *Preliminary Investigation on Battery Sizing Investigation for Thrust Vector Control on Ares I and Ares V Launch Vehicles*, NASA Glenn Research Center, Cleveland, OH, USA, 2011.

[3] H. Kaminaga, J. Ono, Y. Nakashima, and Y. Nakamura, "Development of backdrivable hydraulic joint mechanism for knee joint of humanoid robots," in *Proceedings of the IEEE International Conference on Robotics and Automation*, Kobe, Japan, 12-17 May 2009.

[4] H. Kaminaga, T. Amari, Y. Katayama, J. Ono, Y. Shimoyama, and Y. Nakamura, "Backdrivability analysis of electro-hydrostatic actuator and series dissipative actuation model," in *Proceedings of the IEEE International Conference on Robotics and Automation*, pp. 3–7, Anchorage, AK, USA, May 2010.

[5] Z. Quan, L. Quan, and J. Zhang, "Review of energy efficient direct pump controlled cylinder electro-hydraulic technology," *Renewable and Sustainable Energy Reviews*, vol. 35, pp. 336–346, 2014.

[6] G. K. Costa and N. Sepehri, "Four-quadrant analysis and system design for single-rod hydrostatic actuators," *Journal of Dynamic Systems, Measurement, and Control*, vol. 141, no. 2, Article ID 021011, 2019.

[7] X. L. Shao, J. T. Zhang, and W. D. Zhang, "Distributed co-operative surrounding control for mobile robots with uncertainties and aperiodic sampling," *IEEE Transactions on Intelligent Transportation Systems*, pp. 1–11, 2022.

[8] W. Zhang, X. Shao, W. Zhang, J. Qi, and H. Li, "Unknown input observer-based appointed-time funnel control for quadrotors," *Aerospace Science and Technology*, vol. 126, Article ID 107351, 2022.

[9] Z. Mao, B. Jiang, and P. Shi, "Observer-based fault-tolerant control for a class of networked control systems with transfer delays," *Journal of the Franklin Institute*, vol. 348, no. 4, pp. 763–776, 2011.

[10] L. Y. Hao and G. H. Yang, "Robust fault tolerant control based on sliding mode method for uncertain linear systems with quantization," *ISA Transactions*, vol. 52, no. 5, pp. 600–610, 2013.

[11] L. F. Mendonca, J. M. C. Sousa, and J. M. G. Sá da Costa, "Fault tolerant control using a fuzzy predictive approach," *Expert Systems with Applications*, vol. 39, no. 12, pp. 10630–10638, 2012.

[12] C. H. Houpis and S. J. Rasmussen, *Quantitative Feedback Theory Fundamentals and Applications*, Marcel Dekker, New York, USA, 1999.

[13] O. Yaniv, *Quantitative Feedback Design of Linear and Nonlinear Control Systems*, Kluwer Academic Publishers, Massachusetts, USA, 1999.

[14] M. Karpenko and N. Sepehri, "Robust position control of an electrohydraulic actuator with a faulty actuator piston seal," *Journal of Dynamic Systems, Measurement, and Control*, vol. 125, no. 3, pp. 413–423, 2003.

[15] M. Karpenko and N. Sepehri, "Fault-tolerant control of a servohydraulic positioning system with crossport leakage," *IEEE Transactions on Control Systems Technology*, vol. 13, no. 1, pp. 155–161, 2005.

[16] M. Karpenko and N. Sepehri, "Quantitative fault tolerant control design for a leaking hydraulic actuator," *Journal of Dynamic Systems, Measurement, and Control*, vol. 132, no. 5, pp. 626–634, 2010.

[17] G. Ren, M. Esfandiari, J. Song, and N. Sepehri, "Position control of an electrohydrostatic actuator with tolerance to internal leakage," *IEEE Transactions on Control Systems Technology*, vol. 24, no. 6, pp. 2224–2232, 2016.

[18] G. Ren, J. Song, and N. Sepehri, "Fault-tolerant actuating pressure controller design for an electrohydrostatic actuator experiencing a leaky piston seal," *Journal of Dynamic Systems, Measurement, and Control*, vol. 139, no. 6, Article ID 061004, 2017.

[19] G. Ren, J. Song, and N. Sepehri, "Design of a low-bandwidth position controller based on system identification for an electro-hydrostatic actuator," *Proceedings of the Institution of Mechanical Engineers - Part I: Journal of Systems & Control Engineering*, vol. 232, no. 2, pp. 149–160, 2017.

[20] G. Ren, *Robust Control of Double-Rod and Single-Rod Electrohydrostatic Actuators: Design and Implementation*, Ph.D thesis, Department of Mechanical Engineering, University of Manitoba, Winnipeg, MB, Canada, 2020.

[21] L. Chen and S. Liu, "Fault diagnosis integrated fault-tolerant control for a nonlinear electro-hydraulic system," in *Proceedings of the Conference on Control Technology and Applications*, Yokohama, Japan, 8-10 September 2010.

[22] A. Maddahi, N. Sepehri, and W. Kinsner, "A practical approach for designing fault-Tolerant position controllers in hydraulic actuators: methodology and experimental validation," *Journal of Dynamic Systems, Measurement, and Control*, vol. 142, no. 8, Article ID 081001, 2020.

[23] A. M. Moghaddam, W. Kinsner, G. K. Costa, L. Kumar, K. Butt, and N. Sepehri, "FOPID control with parameter optimization for hydrostatically-actuated autonomous excavators," *IEEE Instrumentation and Measurement Magazine*, vol. 24, no. 2, pp. 109–117, 2021.

[24] G. Ren, G. K. Costa, and N. Sepehri, "Position control of an electro-hydrostatic asymmetric actuator operating in all quadrants," *Mechatronics*, vol. 67, Article ID 102344, 2020.

[25] N. Niksefat and N. Sepehri, "Designing robust force control of hydraulic actuators despite system and environmental uncertainties," *IEEE Control Systems*, vol. 21, pp. 66–77, 2001.

[26] N. Niksefat and N. Sepehri, "A QFT fault-tolerant control for electrohydraulic positioning systems," *IEEE Transactions on Control Systems Technology*, vol. 10, no. 4, pp. 626–632, 2002.